Magnetic Resonance Materials in Physics, Biology and Medicine (2024) 37:53–68
https://doi.org/10.1007/s10334-023-01121-y

RESEARCH ARTICLE

# Subject-specific timing adaption in time-encoded arterial spin labeling imaging

**Nora-Josefin Breutigam[1] · Daniel Christopher Hoinkiss[1] · Simon Konstandin[1,2] · Mareike Alicja Buck[1,3] · Amnah Mahroo[1] · Klaus Eickel[1,2,4] · Federico von Samson-Himmelstjerna[1,3] · Matthias Günther[1,2,3]**

Received: 23 June 2023 / Revised: 18 August 2023 / Accepted: 4 September 2023 / Published online: 28 September 2023


## Abstract

**Objectives** One challenge in arterial spin labeling (ASL) is the high variability of arterial transit times (ATT), which causes associated arterial transit delay (ATD) artifacts. In patients with pathological changes, these artifacts occur when post-labeling delay (PLD) and bolus durations are not optimally matched to the subject, resulting in difficult quantification of cerebral blood flow (CBF) and ATT. This is also true for the free lunch approach in Hadamard-encoded pseudocontinuous ASL (H-pCASL).

**Material and methods** Five healthy volunteers were scanned with a 3 T MR-system. pCASL-subbolus timing was adjusted individually by the developed adaptive Walsh-ordered pCASL sequence and an automatic feedback algorithm. The quantification results for CBF and ATT and the respective standard deviations were compared with results obtained using recommended timings and intentionally suboptimal timings.

**Results** The algorithm individually adjusted the pCASL-subbolus PLD for each subject within the range of recommended timing for healthy subjects, with a mean intra-subject adjustment deviation of 47.15 ms for single-shot and 44.5 ms for segmented acquisition in three repetitions.

**Discussion** A first positive assessment of the results was performed on healthy volunteers. The extent to which the results can be transferred to patients and are of benefit must be investigated in follow-up studies.

**Keywords** Arterial spin labeling · Arterial transit delay artifacts · Free-lunch approach · Time-encoded pCASL · Subject-specific timing

## Introduction

Perfusion is an important parameter for the diagnosis of neurological diseases, which are often accompanied or preceded by changes in blood flow. Arterial spin labeling (ASL) [1] is a noninvasive method for measuring organ perfusion using magnetic resonance imaging (MRI). It uses the arterial blood itself as an endogenous tracer. To this end, ASL uses radio frequency (RF) pulses to magnetically "label" the arterial blood before entering an organ. Thereby allowing the measurement of various hemodynamic parameters such as cerebral blood flow (CBF) (perfusion), arrival times such as arterial transit times (ATT) and arterial blood volume, as well as certain exchange parameters such as vessel wall permeability [2, 3].

There are several ASL techniques [1, 4–6], with pseudocontinuous ASL (pCASL) [7–9] now established as the quasi-standard for steady-state perfusion imaging with ASL [10]. Here, a bolus is created over a period of time (typically 1–3 s) by magnetically labeling blood as it flows through the labling plane outside the imaging volume by locally inverting the magnetization. During a certain delay time, the labeled blood flows downstream and migrates to the tissue [1].

An important physiological parameter for ASL measurements of brain perfusion is ATT. This is the time required for blood to travel from the labeling plane to the imaging voxels

✉ Nora-Josefin Breutigam
nora-josefin.breutigam@mevis.fraunhofer.de

1 Imaging Physics, Fraunhofer Institute for Digital Medicine MEVIS, Max-von-Laue-Str. 2, 28359 Bremen, Germany

2 Mediri GmbH, Heidelberg, Germany

3 Faculty 1 (Physics/Electrical Engineering), University of Bremen, Bremen, Germany

4 Bremerhaven University of Applied Science, Bremerhaven, Germany

of the tissue [11, 12]. ATT is an individual local parameter [13] and therefore important for accurate quantification of absolute CBF [11, 14–16]. If the ATTs are prolonged, artifacts called arterial transit delay (ATD) artifacts may occur [12], complicating correct clinical diagnosis, e.g., in old patients, in patients with ischemic stroke, steno-occlusive disease, or moyamoya disease [11, 12, 17–19]. ATD artifacts are promoted by non-optimal timing of bolus durations (BD) and post-labeling delays (PLD). This is due to the fact that with prolonged ATT, the defined PLD for the image acquisition is too short. The perfusion image then shows a high signal of labeled blood still in the macrovascular phase that has not yet reached the capillary exchange site. Although there are recommended timings for certain age groups and diseases [15], it is not possible to determine the extent to which individual ATTs deviate from these before the start of the acquisition of the perfusion scan. Clinically, information on ATT can be used to detect hemodynamic disturbances in stroke, vascular occlusion or malformations, and aging processes [20]. Several approaches exist to determine ATTs.

A common method for determining ATT is to sample the ASL signal over time and fit a parametric model curve to this sampled data [14]. Such fits yield parameter maps for ATT which can be used to correct CBF values for prolonged ATTs. In classical multi-TI/PLD ASL, multiple images are acquired in multiple measurements each using a different inflow time (TI) or PLD to temporally sample the ASL signal. However, compared to single-TI/PLD-ASL, this approach significantly increases the acquisition time (TA) [21]. Repetitions of the multi-TI/PLD measurement to achieve a sufficiently high signal-to-noise ratio (SNR) further increases the TA. The time constraints of a clinical setup often limit the applicable number of TIs/PLDs, which in turn may reduce the accuracy of quantified perfusion parameters.

Hadamard (or time-encoded) pCASL (H-pCASL) was proposed as a time and temporal SNR efficient multi-TI/PLD technique to accurately sample the ASL signal [22–24]. However, a potential disadvantage of H-pCASL in general is that all N-encoded images are required to decode each perfusion-weighted image (PWI). Artifacts in one or more of the encoded images carry over to all decoded images, potentially leading to erroneous results [21, 25–27]. Furthermore, with standard H-pCASL all N-encoded images have to be acquired before the decoding process of PWIs can be performed. Walsh-Ordered H-pCASL (WH-pCASL) [28] tries to solve this using a specific ordering of the encoding steps such that intermediate PWIs can be decoded even when only early subsets of all N-encoded images are available.

To optimize the timing of the ASL measurement and to obtain ATT information without time penalty and with theoretically the same SNR in CBF maps as in standard pCASL measurements, the so-called "free lunch" (FL) approach for H-pCASL/ WH-pCASL was presented [21]. Here one selects a longer duration and PLD for the first (sub)bolus (further called pCASL-subbolus) than for subsequent subboli (typically, similar to a standard pCASL scan). During the long PLD, the remaining subboli can be generated. This way, not changing the total scan time, a conventional ASL perfusion image resulting from the first bolus and, as a "free lunch", further perfusion images for determining ATT from the remaining subboli and their respective PLDs are obtained.

The approaches described can reduce but not completely eliminate the aforementioned ATD artifacts without extending the times for TI/PLD sufficiently to account for delayed ATTs as a precaution. This would lead to a significant increase in measurement time and would be at the expense of SNR. In the FL approach, for example, the longer pCASL-subbolus image ideally shows a fully perfused brain, while the remaining shorter subboli are used to sample the different inflow phases of the labeled blood on its way to the capillary exchange site. The recommended timings [15, 21] for healthy subjects are adequate in most cases. However, when ATT is prolonged, the pCASL-subbolus image exhibits ATD artifacts. Strategies such as increasing the maximum TI and/or decreasing the pCASL-BD work only to a limited extent because the signal decreases with $T_1$ relaxation, and shortening the pCASL-subbolus degrades the SNR. Therefore, it is desirable to have a pCASL-BD as long as possible, but short enough to avoid ATD artifacts and leave enough time for the remaining subboli. Consequently, it may be advantageous to use individualized timing for each patient to achieve optimal sampling and accurate quantification of CBF.

Early detection of non-optimal timing of BD and PLD is possible with the proposed WH-pCASL, where the first few images already yield usable information. However, PLD, net BD, and individual subbolus durations (SBD) are protocol parameters fixed at sequence start. To obtain optimal results, either a low-resolution pre-scan is required [29] or at least one of these measurement parameters must be changed during runtime. We propose an acquisition strategy allowing automatic adjustment of SBDs during the measurement. This can be performed in a very efficient way.

Preliminary development steps of this work have been presented in abstract form [30–32].

## Theory

This section explains the theoretical background of how automatic adjustment of timing in a time-encoded pCASL acquisition is possible without significantly increasing the measurement time or unnecessarily shortening the pCASL-subbolus.

In Hadamard-encoded pCASL imaging, the long pCASL-bolus (Fig. 1A) is separated into several so-called subboli

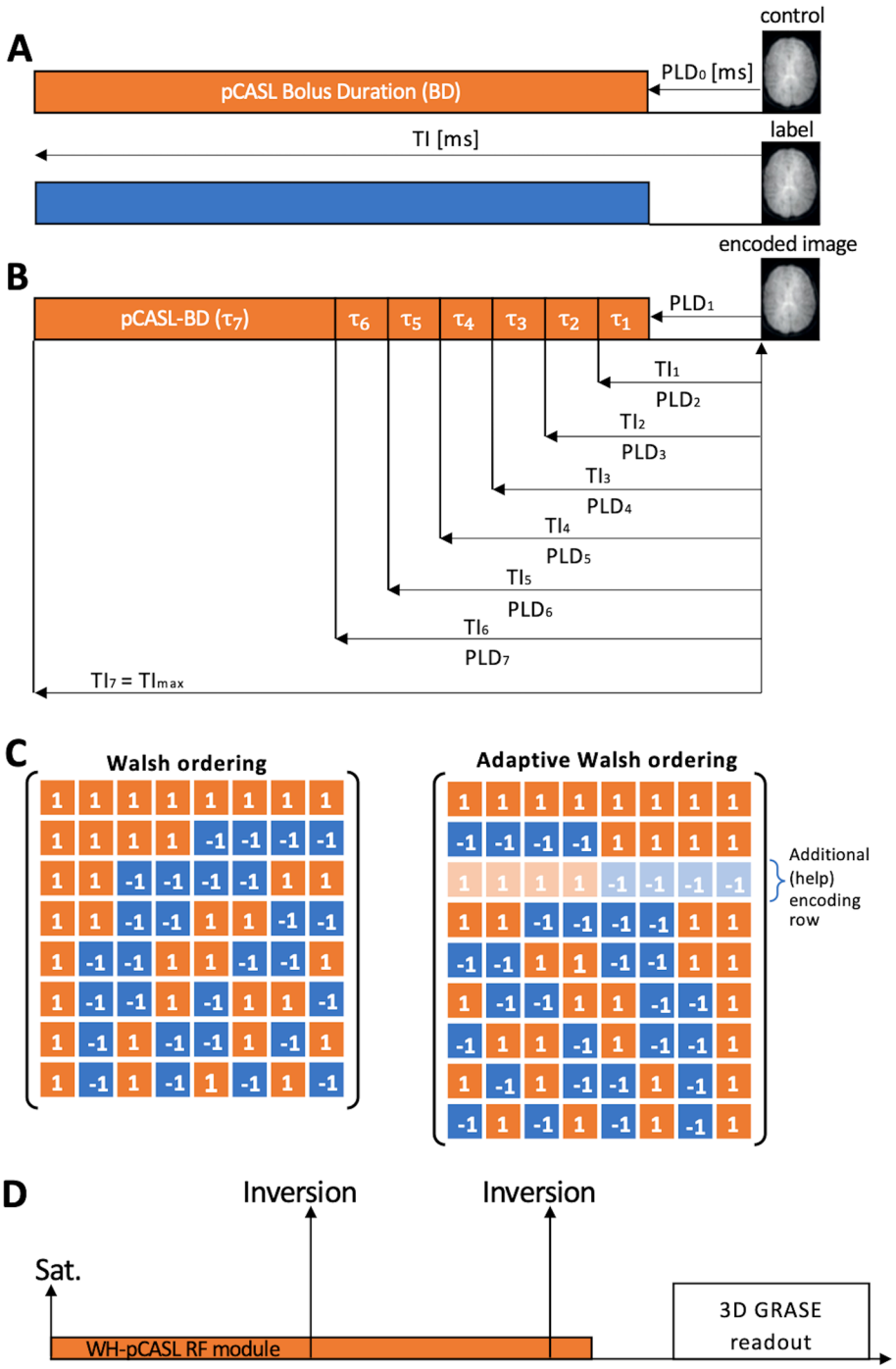


**Fig. 1** **A** Standard pCASL acquisition with long control (orange) and label (blue) bolus. Start $PLD_0$ and pCASL-bolus duration (BD) define the inflow time (TI). **B** Splitting of the longer bolus in multiple sub-boli in a time-encoded pCASL experiment. Each subbolus has a different duration $\tau_i$ ($i = 1–7$), post labeling delay ($PLD_i$) and inflow time ($TI_i$). Again, respective $PLD_i$ and duration $\tau_i$ determine $TI_i$ and vice versa. **C** The conventional Walsh ordering of an $8 \times 8$ Hadamard matrix is converted to the "adaptive" version to facilitate subbolus duration (SBD) adjustments based of intermediate perfusion-weighted images. In addition, the second encoding row is used twice, but with the control ("1") and labeling ("−1") phases reversed. This row is skipped in the final decoding process in which "1" stands for addition and "−1" for subtraction. **D** General sequence scheme with one saturation and two background suppression pulses

(Fig. 1B). Each subbolus can have a different duration $\tau_i$. Consequently, each subbolus has a different $TI_i$ and $PLD_i$ ($i = 1–7$). In the FL-approach the subbolus with the longest inflow time ($TI_{max}$) still represents the long pCASL-(sub) bolus and the remaining subboli are used to sample the inflow of the blood. Accordingly, the blood flowing into the brain is marked with a pattern of label and control states corresponding to the entries of a Hadamard matrix (Fig. 1C). Each entry of "1" or "−1" stands for a subbolus with the status "control" or "label". The perfusion-weighted images (PWI)s with the different TIs can be decoded by adding (1) and subtracting (−1) the encoded images according to the entries of the Hadamard columns.

When Walsh-ordering a natural-ordered Hadamard matrix, the individual rows of the matrix are ordered by their sequence, i.e. the number of sign changes in their entries. Adjacent subboli being in the same phase (label or control) effectively form one combined longer subbolus.

Consequently, the first two rows of any Walsh-ordered Hadamard matrix correspond to a 2×2 natural-ordered one, the first four rows correspond to a 4×4 matrix, the first eight rows correspond to an 8×8 matrix, etc. (compare Fig. 2, Online Resource 1 Figure S2).

It is important to note that within these combined longer partial boluses each individual duration of the shorter subboli is not yet fixed. This degree of freedom is exploited in the adaptive WH-pCASL imaging method. By applying a dedicated encoding matrix (Fig. 1C right), the duration of the subboli, which are decisive for the final pCASL-BD, can be adjusted during active scanning.

## Adaptive bolus duration algorithm

The underlying algorithm is shown in Fig. 2. In each step two intermediate PWIs with different TIs are compared and analyzed during the measurement's runtime to iteratively adapt the pCASL-BD/pCASL-PLD$_7$ while keeping the number of acquisitions as low as possible. Depending on how

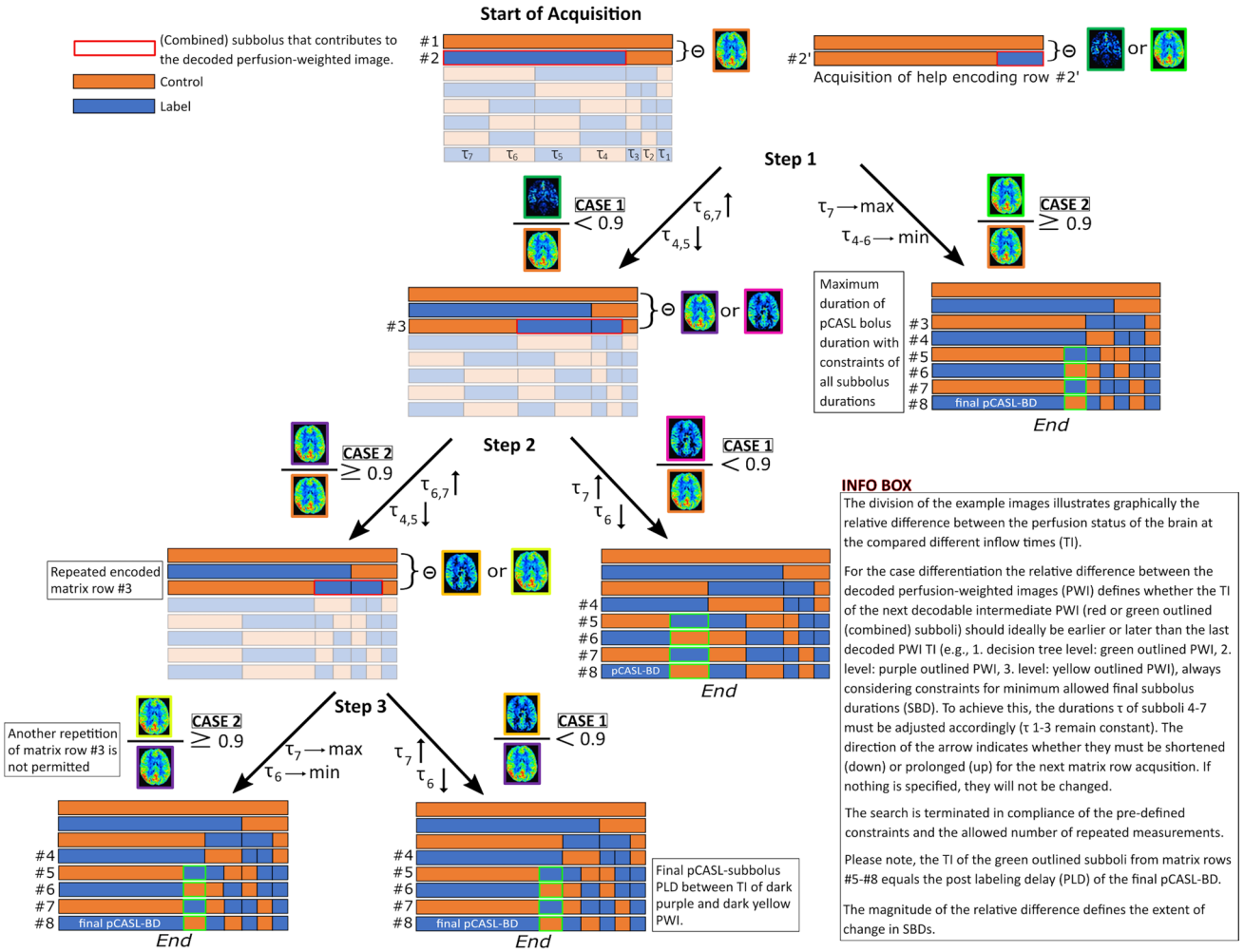


**Fig. 2** The decision tree shows representatively the algorithm for stepwise approximation of an individual final pCASL subbolus duration (SBD) in a time-encoded pCASL measurement using the adapted 8×8 Hadamard encoding matrix (only 7 SBDs shown here because the 8th column does not result in a perfusion-weighted image (PWI)). Crucial to the algorithm is the fact that neighboring subboli with the same label or control state can be combined into longer subboli. Within these combined subboli, the subsequent borders for a change of label and control are not yet fixed. This results in initial matrices with smaller dimensions, which can be used for the calculation of here so-called intermediate PWIs. After the initial 2×2 acuqisition (#1 and #2) and using the help encoding row (#2′) PWIs with the longest inflow time (TI) (orange PWI) and with an earlier TI (green PWIs) can be calculated. Depending on the subject measured, the earlier PWIs may show a brain with more (dark green PWI) or less (light green PWI) labeled blood inside. Then, the ratio of the number of voxels above the noise threshold is determined and compared in a complete image volume of PWIs (only one slice is shown here as an example). Depending on the ratio, the SBDs of the next Hadamard matrix encoding row(s) are adjusted (see Info Box). The exact calculations of the SBDs can be found in Online Resource 2. Depending on the result of the PWI comparison and the previously defined allowed maximum and minimum duration of each subboli, individual rows are adjusted, repeated or the measurement is terminated with adjusted SBDs by including all subsequent matrix rows accordingly

much blood is supplied to the brain in each intermediate PWI, the SBDs of the subsequent matrix rows are either shortened or prolonged.

At the beginning of the algorithm $TI_{max}$ and the first $PLD_1$ are set (Fig. 2, Start of Acquisition). These parameters cannot be changed during the runtime of the measurement. Furthermore, the start SBDs are defined, whereby only the inflow time $TI_3$ (first change between label and control state in #2 & #2′) is fixed at this stage (Figs. 1B, C, 2, acquisition of help encoding row). Moreover, the SBDs $\tau_{1-3}$ remain constant throughout the duration of the acquisition.

After the acquisition of further encoding matrix rows (Fig. 2, Step 1–3), it can be seen that with each additional row of the encoding matrix, further (combined) subboli are given fixed durations that cannot be changed during the acquisition of subsequent matrix rows. Whenever there is a change between label and the control state, the corresponding TI is fixed for the course of the experiment. If this defined TI is to be changed, the acquisition of the corresponding row in the encoding matrix must be repeated. This results in the essential property of the presented algorithm. The duration of the final pCASL-subbolus ($\tau_7$) and thus the decoded PWI can not be investigated with the acquisitions of single encoding matrix rows. With the 8 × 8 encoding matrix used, the pCASL-subbolus PWI can only be decoded when all eight matrix rows have been successfully acquired. As a result, a stepwise adaptation to a final pCASL-$PLD_7$ is performed during the experiment by comparing PWI with earlier TI with PWI with later TI and adjusting the individual SBDs in the subsequent matrix rows accordingly. Within few iteration steps, a more "optimized" SBD of the final pCASL-subbolus can thus be approximated.

The number of adjustments is limited by the size of the used encoding matrix, which is two for an 8 × 8 Hadamard acquisition matrix.

All decisions are based on the "degree of filling" of the brain. If the brain is still sparsely filled, it is assumed that labeled blood continues to be in the macrovascular phase. Therefore, for the comparison, the number of voxels having signal values above the noise level of the PWI is calculated. The histogram of each image slice is used to calculate the respective noise level. Here, the observation is exploited that the number of "filled" voxels (NoV) increases with TI (Online Resource Figure S1), at least until venous outflow and/or until SNR decreases too much. To compare the NoV in the complete image volume of two PWIs, the ratio between them is calculated, e.g., in Step 1 (Fig. 2):

$$R_{\mathrm{rel},1} = \frac{\mathrm{NoV}\left(\mathrm{PWI}_{\mathrm{TIearly}}\right)}{\mathrm{NoV}\left(\mathrm{PWI}_{\mathrm{TImax}}\right)}.$$

A threshold value is used as a criterion for adjusting the SBDs to reduce potential ATD artifacts in the final pCASL-subbolus PWI. If $R_{\mathrm{rel}} <$ threshold, the potential final pCASL-BD has to be shortened. If $R_{\mathrm{rel}} \geq$ threshold, the potential final pCASL-BD has to be prolonged, which means a repeated acquisition of the previous matrix row with adapted timings is necessary. $R_{\mathrm{rel}}$ is used for the calculation of the adapted SBDs as well.

In the following, the flow of the algorithm is explained step by step on the basis of Fig. 2.

**Step 1:**

Since only one PWI can be calculated with the first two encoded images, an auxiliary row with an interchanged label and control state of the second matrix row is included accordingly (#2′). This row is skipped in the final decoding process. Two PWIs, one with $TI_{max}$ (PWI#1, orange) and one with an earlier TI (PWI#2, green) can then be compared.

If $R_{\mathrm{rel},1} \geq$ threshold (CASE 2), the brain is already perfused early. To increase the SNR of the final pCASL-subbolus, the final pCASL-BD should become maximally long (minimum PLD) and all other subboli being given a minimum duration within defined limits. All remaining matrix rows are acquired and no further adjustments are made. Any adjustment is made within a defined allowed minimum and maximum durations for the last pCASL-subbolus and the remaining subboli (see "Methods" section).

If $R_{\mathrm{rel},1} <$ threshold (CASE 1), the brain is not as much perfused in PWI#2 than in PWI#1. To reduce potential ATD artifacts in the final pCASL-PWI, the third matrix row (#3) is acquired with adapted subboli durations. The relative difference in the number of filled voxels defines how long the individual (combined) subboli in this matrix row become:

$$\mathrm{SBD}_{\mathrm{pCASL,init}} = \sum_{i=4}^{7} \tau_i$$

$$\mathrm{SBD}_{\mathrm{pCASL,new}} = R_{\mathrm{rel},1} \times \mathrm{SBD}_{\mathrm{pCASL,init}}$$

$$\tau_{7,\mathrm{new}} = \frac{\mathrm{SBD}_{\mathrm{pCASL,new}}}{2}$$

$$\tau_{6,\mathrm{new}} = \frac{\mathrm{SBD}_{\mathrm{pCASL,new}}}{2}$$

$$\tau_{5,\mathrm{new}} = \frac{\mathrm{SBD}_{\mathrm{pCASL,init}} - \mathrm{SBD}_{\mathrm{pCASL,new}}}{2}$$

$$\tau_{4,\mathrm{new}} = \frac{\mathrm{SBD}_{\mathrm{pCASL,init}} - \mathrm{SBD}_{\mathrm{pCASL,new}}}{2}$$

$$\tau_{1-3,\mathrm{new}} = \tau_{1-3,\mathrm{old}}$$

**Step 2:**

The first and third matrix rows (#1 and #3) can be used to decode another intermediate PWI (PWI#3) (outlined in purple). Depending on the state of perfusion at this TI, $R_{rel,2}$ < threshold (CASE 1) or ≥ threshold (CASE 2). In CASE 1, the brain is less perfused in PWI#3 than in PWI#1. Therefore, the acquisition of the following matrix rows continues with adapted SBDs depending on $R_{rel,2}$:

$$SBD_{pCASL,old} = \tau_{6,old} + \tau_{7,old}$$

$$\tau_{7,new} = SBD_{pCASL,old} \times R_{rel,2}$$

$$\tau_{6,new} = SBD_{pCASL,old} - \tau_{7,new}$$

$$\tau_{1-5,new} = \tau_{1-5,old}$$

With $\tau_{old} = \tau_{new}$ from Step 1.

Since the final duration of the pCASL subbolus is already defined in these matrix rows, all further matrix rows are acquired accordingly and the measurement is completed.

In CASE 2, the brain in PWI#3 is comparably perfused to PWI#1. To achieve the highest possible SNR in the final pCASL-subbolus, the third matrix row (#3) should be acquired again with appropriately adjusted SBDs. The new TI of the decodable PWI#3′ (yellow) lies exactly between the TI of PWI#2 and PWI#1.

**Step 3:**

In Step 3, the newly decoded PWI#3′ (yellow) is compared with the old PWI#3 (dark purple) from CASE 2 in Step 2. In CASE 1, PWI#3′ is less perfused than PWI#3, so the final pCASL-PLD should be between the two compared PWIs, again depending on the relative difference in perfusion.

In case 2, PWI#3′ shows a comparable perfusion status to the old PWI#3, suggesting that the final pCASL-subbolus might even be longer with a low probability of ATD artifacts. Since another repetition of matrix row #3 is not allowed to keep acquisition time as low as possible, the final pCASL-BD is acquired as long as possible, considering the minimum allowed SBD for the adjacent subbolus ($\tau_6$).

A run-through of the algorithm with example start and end values for SBDs in the schematic of Fig. 2 can be found in Online Resource 1 Figure S3. The complete algorithm with calculations of all SBDs can be found in Online Resource 2.

## Methods

### Data acquisition

Five healthy volunteers (aged 21–57 years; one male) were scanned with a 3-Tesla MR-system (MAGNETOM Skyra, SIEMENS Healthineers AG, Erlangen, Germany) and a 20-channel head coil. Written informed consent was obtained before measurements, and the study was conducted according to a general protocol for the development of pulse sequences approved by the local ethics committee.

All subjects were scanned with a measurement protocol consisting of a three-dimensional $T_1$-weighted gradient-echo acquisition (MPRAGE), time-of-flight (TOF), $M_0$ and multiple ASL measurements performed in a single-shot (ss) and segmented (seg) acquisition scheme.

During acquisition, the intermediate PWIs were processed with the in-house developed processing program in the manufacturer's own image calculation environment (ICE). The calculated adjustments for the SBD timings for the subsequent encoding matrix row were fed back to the sequence, where the SBDs were then adjusted during runtime.

### Time of flight angiography

For positioning the labeling slab accurately, a low-resolution TOF angiogram of the lower head and neck was acquired. The labeling plane was located as perpendicular to the carotid and vertebral arteries as anatomy allows, which is normally shortly upstream the V3-segment of the vertebral arteries. Sequence parameters were: field of view (FOV) = 200 × 150 × 76 mm$^3$, matrix size: 256 × 192 × 76 (interpolated to 512 × 384 × 76), partial Fourier = 7/8, TR/TE = 21/3.48 ms, acquisition time (TA) = 1:02 min.

### 3D GRASE

For all image acquisitions for the ASL MR-scans an identical ss or seg three-dimensional (3D) gradient and spin echo (GRASE) readout was used [33]. Sequence parameters were: FOV = 256 × 192 × 96 mm$^3$, matrix size: 64 × 48 × 24 (interpolated to 128 × 96 × 24), four segments (seg), turbo factor = 24 (ss), turbo factor = 12 (seg), echo planar imaging factor = 48 (ss), echo planar imaging factor = 24 (seg), receiver bandwidth = 2298 Hz/pixel, flip angle (refocusing pulse) = 120°, TE = 29.5 ms (ss), TE = 18 ms (seg).

### $M_0$ images

For quantification purposes, three $M_0$ images with different TIs [400, 1700, 3000] ms were acquired. Images were acquired using a slab-selective saturation recovery method with the same 3D GRASE reading procedure used for the WH-pCASL measurements.

### Background suppression

For all ASL acquisitions, background suppression was used. After a saturation module, two hyperbolic secant pulses (ß = 800 $s^{-1}$, μ = 24.0) [34] were applied during the encoding phase (compare Fig. 1C). The timings $\theta_1$ and $\theta_2$ of the two inversion pulses were calculated using an analytical solution for nulling components with relaxation times $T1_{opt}$ = 700 ms and $2 \times T1_{opt}$ = 1400 ms [33]. The label/control condition was inverted after every inversion pulse as described in [24]. Prior to the 3D GRASE readout, tissue signal outside the imaging slab is nulled with multiple modulated saturation pulses [33].

### Fixed WH-pCASL

The 8 × 8 Walsh-ordered Hadamard matrix [28] (Fig. 1A) was used as an encoding scheme. For these acquisitions with fixed predefined SBDs, the different scenarios are listed in Table 1. The timing with intentionally too-long pCASL-BD/too-short pCASL-PLD for healthy subjects was chosen to simulate ATD artifacts in the pCASL-subbolus PWI. With TR = 5000 ms and one preparation scan, respectively, the durations for these acquisitions were TA = 0:45 min (ss) and TA = 2:45 min (seg).

### Adaptive WH-pCASL

The proposed adaptive 8 × 8 Walsh-ordered matrix with an additional help encoding row (Fig. 1A) was used as an encoding scheme.

Three repeated measurements were performed for each of the adaptive WH-pCASL acquisitions to test the robustness of the algorithm. Each repetition had the same starting values and the algorithm adjusted the imaging timings, respectively. For the adaptive measurements that were compared with the quantification results of the measurements with fixed SBDs, the initial duration of each subbolus is listed in Table 1. The first two rows of the encoding matrix are acquired with these values. As additional encoding rows are acquired, the SBDs are adjusted accordingly. With TR = 5000 ms and one preparation scan, respectively, the durations for these acquisitions were TA = 0:50 min (+ 5 s if one encoding row has to be repeated) (ss) and TA = 3:05 min (+ 20 s if one encoding row has to be repeated) (seg).

In addition, the behavior of the algorithm presented here was tested with changed start values for $PLD_1$ and max TI's for ss only (compare Online Resource 1 Table S1). With TR = 5500 ms and one preparation scan, each TA = 0:55 min (+ 5.5 s if one encoded row is repeated).

### Adaption constraints

The threshold for the relative difference in NoV ($R_{rel}$), which determines whether the pCASL-BD must be shortened or lengthened, was set at 10%. Experimentally, this number has proven to be appropriate.

Since the signal of the subboli depends on $T_1$ relaxation effects, subboli with a longer TI lose more signal than boli with a shorter TI. Therefore, certain minimum allowable SBDs were defined in the algorithm for each subbolus. For

**Table 1** Different timing scenarios for standard WH-pCASL and the start values for adaptive WH-pCASL

| Fixed WH-pCASL (ss and seg) | | | | |
|---|---|---|---|---|
| | Max TI [ms] | pCASL-BD $\tau_7$ [ms] | pCASL-PLD [ms] | SBDs [ms] (subbolus $\tau_{6-1}$) |
| Recommended pCASL-PLD/pCASL-BD* | 3600 | 1800 | 1800 | (500, 240, 240, 240, 240, 240) |
| pCASL-BD too short/pCASL-PLD too long | 3600 | 1000 | 2600 | (500, 400, 400, 400, 400, 400) |
| pCASL-BD too long/pCASL-PLD too short | 3600 | 2600 | 1000 | (150, 150, 150, 150, 150, 150) |
| Adaptive WH-pCASL (ss and seg) | | | | |
| | Max TI [ms] | pCASL-BD [ms] | pCASL-PLD [ms] | SBDs [ms] (subbolus $\tau_{7-1}$) |
| Start values | 3600 | To be estimated during runtime | To be estimated during runtime | (695, 695, 695, 695, 240, 240, 240) |

*ss* single-shot, *seg* segmented, *PLD* post labeling delay, *TI* inflow time, *BD* bolus duration, *SBD* subbolus duration

*White paper recommendation for healthy subjects aged < 70 years [15] and with T1 relaxation adapted BDs after[21]

this work, the minimum allowed pCASL-BD ($\tau_7$) was set to 1000 ms, the minimum allowed SBD for the subbolus ($\tau_6$) before the pCASL-subbolus was limited to 300 ms, and the next two subboli ($\tau_{5-4}$) had to have a minimum duration of 200 ms. In addition, to keep the total scan time low and the measurement as efficient as possible, only one repeated acquisition of encoding row #3 was allowed.

## Image analysis

### Evaluation of the robustness of the adaption algorithm

The final adjusted SBDs and pCASL-BDs/PLDs from the three repeated measurements, each performed in the ss- and seg-data acquisition schemes were compared within-subject and between-subjects. Standard deviations within-subject and between-subjects (even when the number of subjects and repeats was relatively small) were used as the method of evaluation. A one-way ANOVA test was performed to quantify the inter-subject dependency.

In addition, the pCASL-subbolus PWI and the preceding PWI from subbolus $\tau_6$ were visually inspected to determine whether in this PWI the brain was already completely filled with labeled blood or whether, for instance, the outer brain areas were not yet perfused.

### Calculation of CBF and ATT maps

The decoded PWIs were processed using the Oxford Centre for Functional MRI of the Brain (FMRIB) software library (FSL) [35]. Structural data were processed using the fsl_anat pipeline. Whole-brain masks and gray and white matter probability maps (GM, WM) were used to mask the voxels of interest. Voxel-wise fitting was performed within the whole-brain mask using the underlying two-compartment model in FSL. $M_0$ map was calculated by applying a mono-exponential non-linear least squares fit using the Python function curve_fit from the Scipy.Optimize library. The result was fed into the FSL quantification pipeline. The calculated mean CBF and ATT values with their corresponding standard deviations as an indicator of the uncertainty of the performed fit were then compared for GM and WM with the different WH-pCASL timings and the adaptive WH-pCASL results.

### Analysis of ATD artifacts

The final pCASL-subbolus PWIs with different PLDs were visually examined for hyperintense regions as signs of macrovascular signal. In addition, the mean and median of the image histograms were determined and compared between the different timings. The higher the difference, the more "outliers" of voxel signal values that could indicate hyperintense signal and thus the presence of ATD artifacts presumably exist.

In the measurements with a pCASL-PLD$_7$ = 1000 ms, ATD artifacts are likely to be present in healthy subjects [36]. The distance between mean and median in the histogram of these images can therefore serve as a landmark for the results with other timings.

## Results

Table 2 shows the resulting pCASL-subbolus PLDs for all five volunteers and three repetitions of the same measurement. The mean standard deviations of the final intra-subject pCASL-PLD$_7$ are 38.5 ms (ss) and 36.33 ms (seg). In comparison, the mean standard deviation of the final inter-subjects pCASL-PLD$_7$ are 122.87 ms (ss) and 127.87 ms (seg). The mean difference between adaption results for pCASL-PLD$_7$ from ss and seg acquisition is 50.47 ± 9.84 ms.

For 3 of 5 subjects, the algorithm repeated the acquisition of matrix encoding row #3 once per measurement.

Figure 3 compares an example adaption result with the recommended [15, 21] but not optimized and non-optimal timings for healthy subjects. On visual inspection, it can be seen that timing with the pCASL-BD = 1000 ms has a low signal and the brain is already fully perfused in early subboli. Timing with the pCASL-BD = 2600 ms shows an insufficient sampling of the early subbolus and hyperintense signal in the pCASL-subbolus PWI.

Figure 4A shows the mean CBF and ATT results of all ss-experiments in GM and WM with their associated standard deviations. For illustration purposes, the standard deviations can be directly compared in Fig. 4B. The same is shown for all experiments with the seg-acquisition scheme in Fig. 5A, B.

In Fig. 6, the pCASL-subbolus PWI can be compared visually with the preceeding PWI in three of five subjects. The focus is on the perfusion status in the outer brain regions. It also allows visual inspection and comparison of potential ATD artifacts in suboptimal timings (e.g., arrow in PWI pCASL-BD = 2600 ms).

The quantitative results of a preliminary analysis for ATD artifacts are compared in Fig. 7. For this purpose, a normalized difference between the mean value of the pCASL-subbolus PWI histogram and the median value is calculated for all timings and subjects.

Finally, Fig. 8 shows the PWI (three out of 24 slices) for the adapted pCASL-PLD$_7$ and the corresponding CBF and ATT maps.

Additionally, in Online Resource 1 Table S2 the adjustment results for all subjects with different starting values of PLDs and TI$_{max}$ can be found. At TI$_{max}$ = 4600 ms and a start PLD$_1$ of 100 ms, the final pCASL-PLD$_7$ was set exactly or

**Table 2** Adapted pCASL-subbolus post labeling delay (PLD) [ms] (all subjects)

| Subject | 1 | 2 | 3 | 4 | 5 | |
|---|---|---|---|---|---|---|
| Max TI = 3600 ms | start PLD = 100 ms | | | | | |
| Single-shot acquisition adapted pCASL-subbolus PLD [ms] | | | | | | |
| Rep 0 | 1781 | 1520 | 1807 | 1833 | 1898 | |
| Rep 1 | 1731 | 1520 | 1824 | 1815 | 1927 | |
| Rep 2 | 1757 | 1636 | 1639 | 1787 | 1893 | |
| Mean | **1756.33** | **1558.67** | **1756.67** | **1811.67** | **1906.00** | |
| SD | **20.42** | **54.68** | **83.49** | **18.93** | **14.99** | |
| p (one-way ANOVA)/Mean SD intra-subject | < 0.001 | | | | | 38.5 |
| SD inter-subjects (all repetitions) | | | | | | **122.87** |
| Segmented acquisition adapted pCASL-subbolus PLD [ms] | | | | | | |
| Rep 0 | 1816 | 1520 | 1871 | 1757 | 1808 | |
| Rep 1 | 1877 | 1520 | 1800 | 1753 | 1830 | |
| Rep 2 | 1748 | 1520 | 1736 | 1727 | 1946 | |
| Mean | **1813.67** | **1520.00** | **1802.33** | **1745.67** | **1861.33** | |
| SD | **52.69** | **0.00** | **55.14** | **13.3** | **60.54** | |
| p (one-way ANOVA)/Mean SD intra-subject | < 0.001 | | | | | 36.33 |
| SD inter-subjects (all repetitions) | | | | | | **127.87** |
| Absolute difference single-shot—segmented [ms] | | | | | | |
| Single shot mean | 1756.33 | 1558.67 | 1756.67 | 1811.67 | 1906.00 | |
| Segmented mean | 1813.67 | 1520.00 | 1802.33 | 1745.67 | 1861.33 | |
| Absolute difference | **57.33** | **38.67** | **45.67** | **66.00** | **44.67** | |
| Mean difference | | | | | | 50.47 |
| SD | | | | | | **9.84** |

For derived values, i.e. bold values in last column and 3rd last row, statistical testing is not beneficial

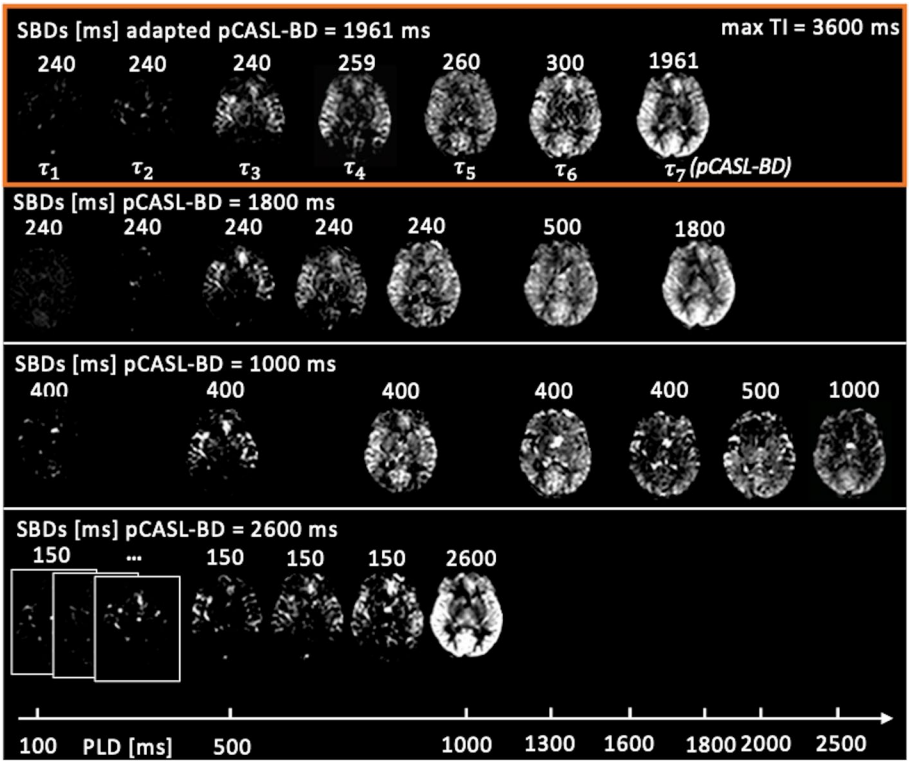


**Fig. 3** Comparing four different timings, the resulting sampling of the inflow of labeled blood for one subject is shown. Each timing option (from top to bottom): (1) automatically adapted pCASL bolus duration (BD) (adapted pCASL-BD = 1961 ms), (2) pCASL-BD = 1800 ms (recommended [15, 23]), (3) pCASL-BD = 1000 ms (intentionally too short), (4) pCASL-BD = 2600 ms (intentionally too long) has different effective bolus post labeling delays (PLD) and subbolus durations (SBD) ($\tau_{1-7}$)

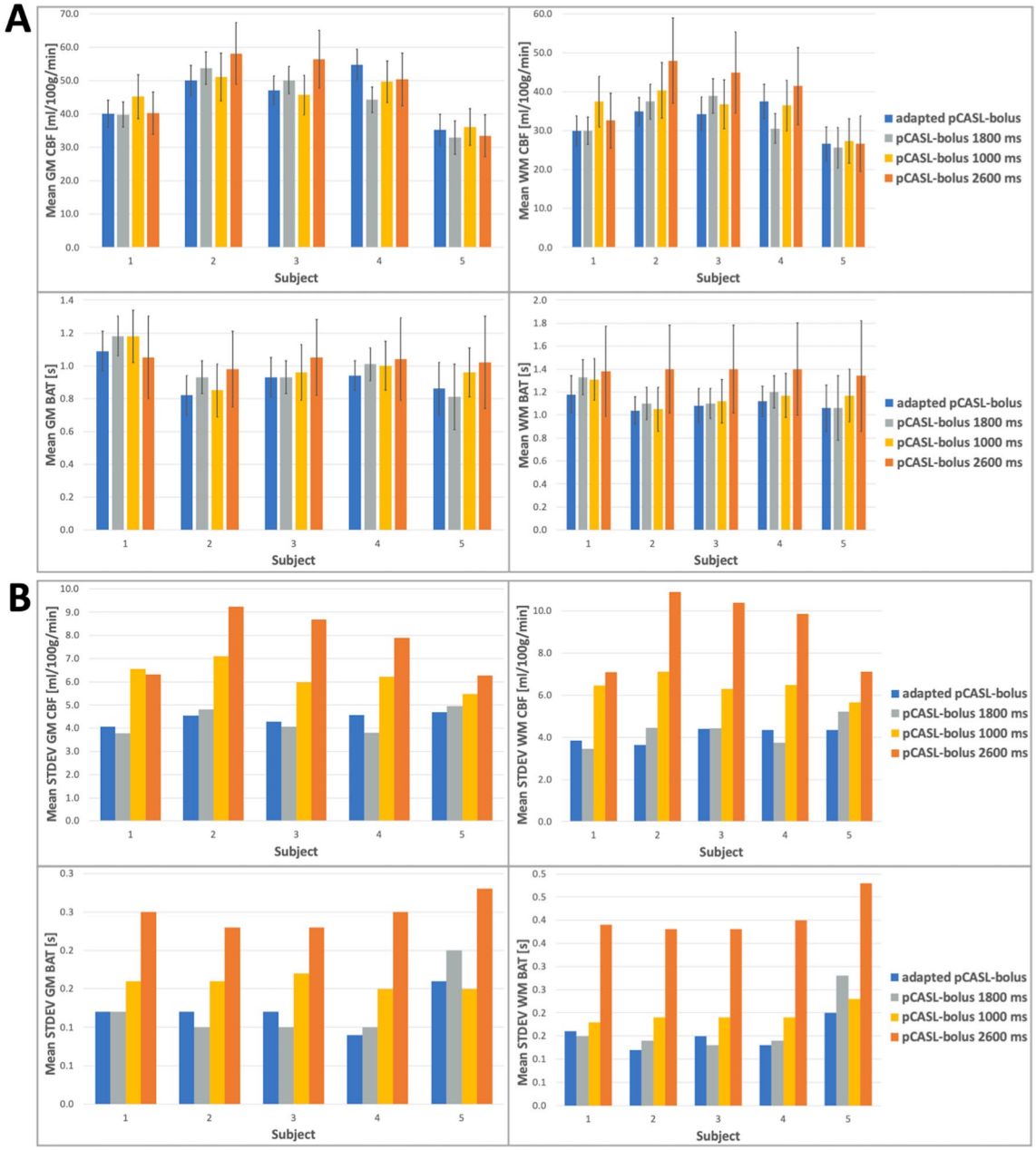


**Fig. 4** **A** The mean quantification results for CBF and ATT in the gray and white matter (GM, WM) from the single-shot acquisitions are shown for the four different timing options and all subjects. **B** The respective mean standard deviations as a measure of uncertainty in the quantification results are plotted side-by-side to compare the influence of sampling on confidence in the quantification results. The final adjusted pCASL-subbolus durations from the adaption process are: 1843 ms (subject 1), 1964 ms (subject 2), 1961 ms (subject 3), 1813 ms (subject 4), 1673 ms (subject 5)

close to its minimum allowed duration within the predefined constraints for SBDs (see "Methods" section). The same is true for the next setting with a start $PLD_1$ of 1100 ms. For the measurements with $TI_{max} = 2600$ ms, the maximum possible pCASL-$PLD_7$ would have been 1600 ms. The algorithm ended here in one of the three repetitions in subject 1 and was closed once in subject 5. All other results ended at the minimum allowed $PLD_7$ of 1520 ms.

## Discussion

In this paper, a possible technical solution for subject-specific adjustment of SBDs during the runtime of a measurement with acceptable time loss is presented. The technical feasibility is evaluated to possibly find an optimized pCASL-BD/PLD for presumptive avoidance of ATD artifacts in time-encoded ASL measurements. The method has not yet been tested in patients,

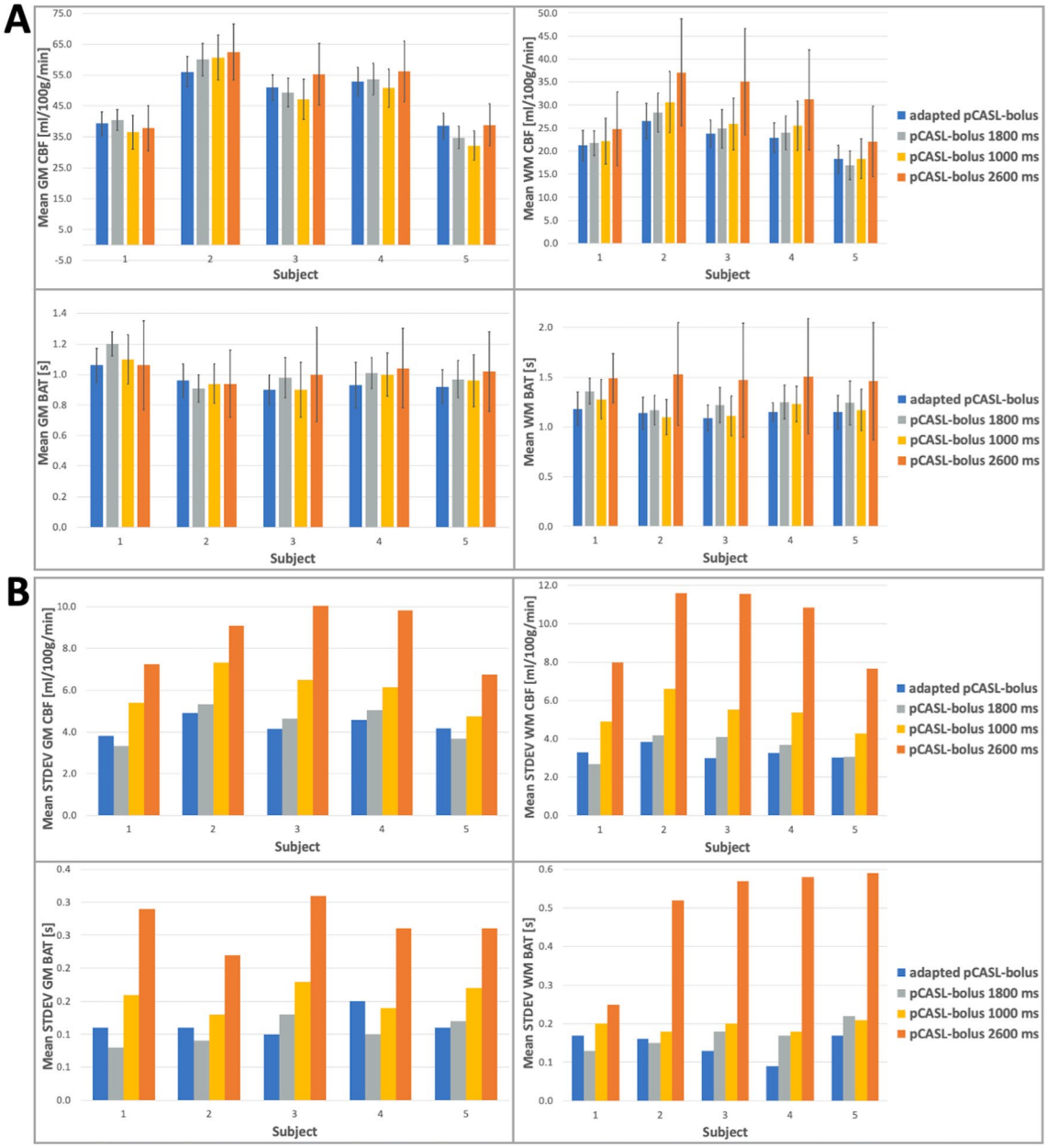


**Fig. 5** **A** Same as in Fig. 4, but here the mean quantification results for CBF and ATT in the gray and white matter (GM, WM) from the segmented acquisitions are shown for the four different timing options and all subjects. **B** The respective mean standard deviations as a measure of uncertainty in the quantification results are plotted side-by-side to compare the influence of sampling on confidence in the quantification results. The final adapted pCASL bolus durations from the adaption process are: 1852 ms (subject 1), 2080 ms (subject 2),1864 ms (subject 3), 1843 ms (subject 4), 1654 ms (subject 5)

therefore no statement can be made about an actual reduction of ATD artifacts in the case of prolonged ATTs.

## Evaluation of the robustness of the adaption algorithm

The proposed time-encoded ASL adaption algorithm consistently found individual timings for the SBDs and pCASL-BDs. In the three repetitions, a relatively low intra-subject standard deviation can be observed, which suggests a robust performance and good repeatability of the proposed approach. Additionally, the standard deviation within a subject was smaller than the standard deviation between subjects for both ss- and seg-acquisition (see Table 1). This may indicate that the algorithm adjusts the SBDs according to individual inflow behavior, which varies among healthy

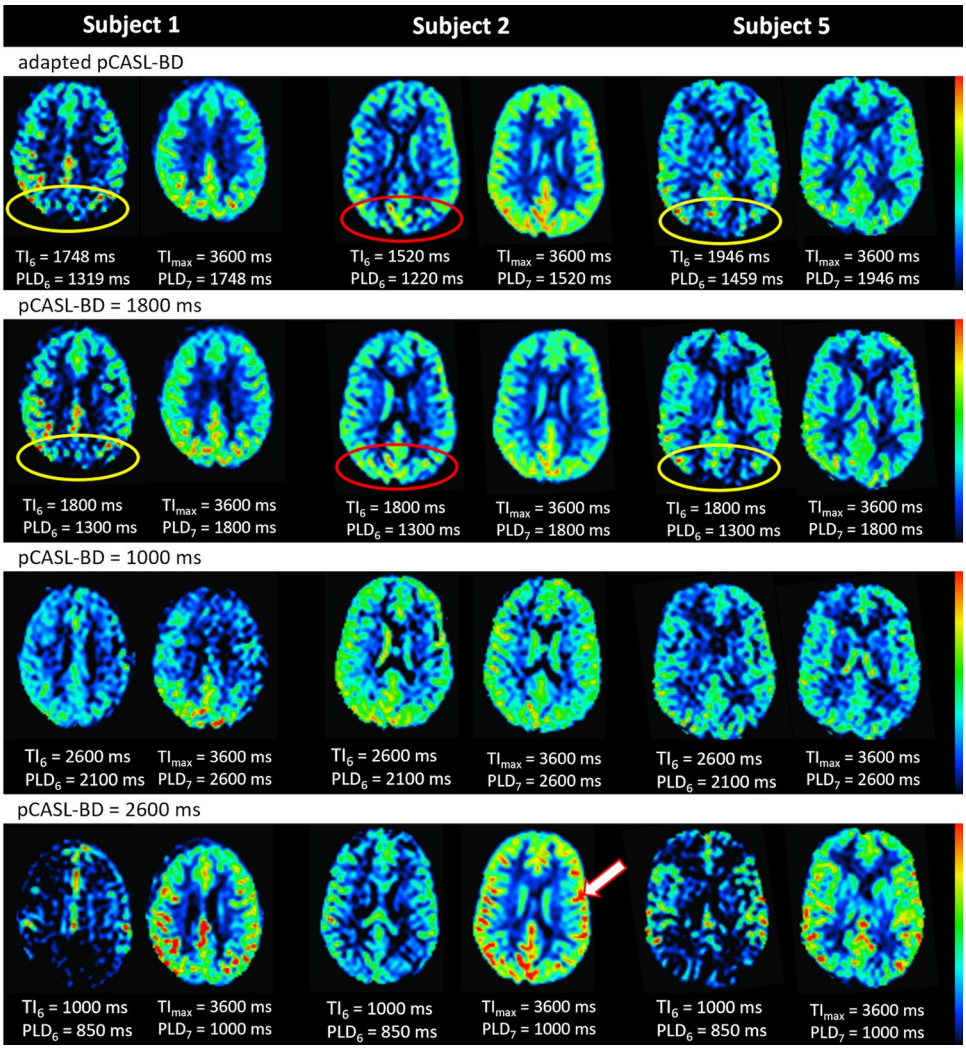


**Fig. 6** Shown are the perfusion-weighted images (PWI) of the long pCASL-subbolus (right) and the preceding subbolus (left) of three of the five subjects. The first row shows the results of the adaption, the second shows the recommended timing with pCASL bolus duration (BD) = 1800 ms, and the third and fourth show the suboptimal timing with pCASL-BD = 1000 ms and pCASL-BD = 2600 ms, respectively. With the adjusted timing, the brain is already almost completely perfused at the inflow time (TI) before the pCASL-subbolus, except for the outer brain region (see yellow and red circles). The recommended timing was also optimal for subjects 1 and 5, but not ideal for subject 2 (red circle), where the brain was already fully perfused at $TI_6$. The third row shows a fully perfused brain at both TIs. The fourth row shows hyperintense signals in the pCASL-subbolus PWI, indicating the presence of intravascular signal

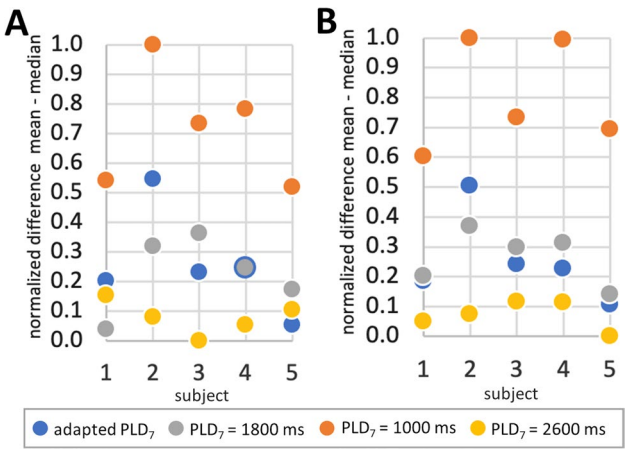


**Fig. 7** The normalized difference between the mean and median values obtained from the histograms of the perfusion-weighted images decoded from the pCASL-subbolus are compared for all timings and subjects as an indicator of the presence of hyperintense signals. **A** Results of single-shot acquisition, **B** results of segmented acquisition

subjects in general and changes with gender and age [11, 13, 15, 16, 37]. The algorithm logically adjusted the SBDs differently for each subject but within the range of expected normal inflow behavior in healthy subjects. Except for subject 2, the adjusted pCASL-$PLD_7$ values were all within the range of recommended times for healthy subjects aged < 70 years [15, 21]. For subject 2, the algorithm chose the smallest pCASL-$PLD_7$ that was possible within the preset adaption restraints. Figure 6 (red circle) shows that the brain was indeed already almost completely filled at the TI before the pCASL-subbolus. In comparison, the TI before the recommended pCASL-$PLD_7$ (= 1800 ms) already shows a well-filled brain, even in the outer brain regions. Therefore, the results suggest that subject 2 indeed had a faster inflow response than the other four subjects.

The measurements in the ss-acquisition scheme have a much shorter scan time than the segmented measurements. However, the image quality is inherently lower. It is also noted that the mean difference between the adaption results for pCASL-$PLD_7$ between the two schemes is higher than

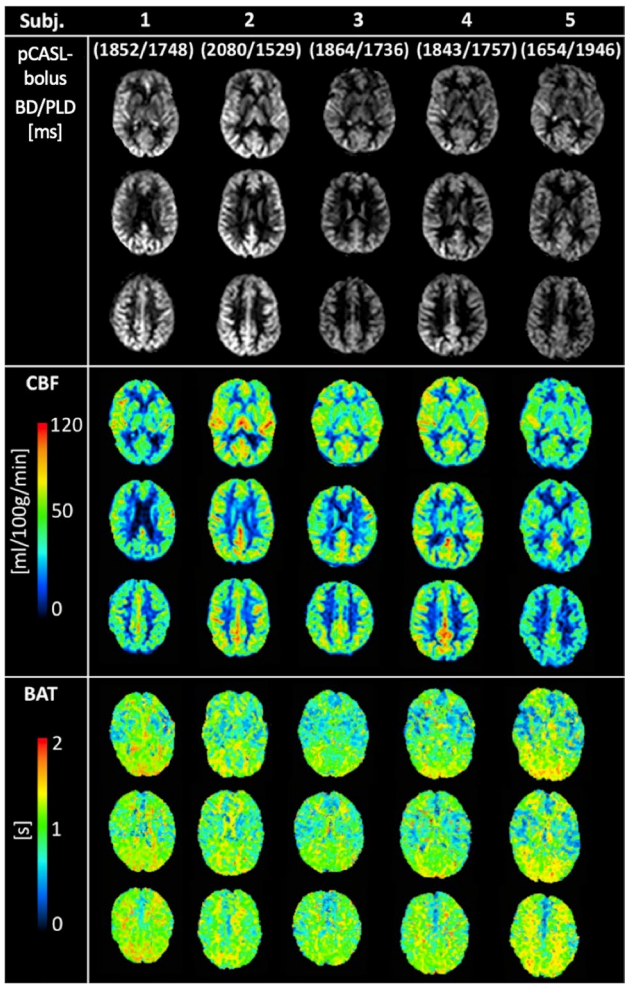


**Fig. 8** Results of adapted timing with respective pCASL bolus duration (BD) and its effective post-labeling delay (PLD) for all subjects. Three out of 24 slices from the perfusion-weighted images, the respective CBF maps [ml/100 g/min] and the ATT maps [s]

the measured standard deviation between three repetitions within a subject. However, the short measurement time of the ss-data could be advantageous in routine clinical practice or serve as a calibration measurement before another, possibly more advanced ASL measurement like a multi-TE measurement to determine the integrity of the blood–brain barrier [38]. In this case, even lower resolution would be conceivable because the calibration perfusion data would not subsequently be used for quality determination and diagnosis.

When different starting values were selected for $PLD_1$ and $TI_{max}$ (see Online Resource 1 Table S1), the algorithm adjusted the SBDs and the pCASL-$PLD_7$ accordingly within the predefined constraints on the minimum allowable SBDs (compare Online Resource 1 Table S2). Thus, with a longer $TI_{max}$ of 4600 ms and a relatively late $TI_3$ of 1300 ms, the algorithm consistently adjusted the pCASL-$PLD_7$ to the minimum allowable value of 2000 ms, except for subject 1, indicating that the algorithm automatically recognized that the brain was perfused at an earlier TI and therefore adjusted the pCASL-subbolus to the maximum possible duration to obtain the highest possible SNR. $TI_3$ defines the inflow time of the second decoded PWI (outlined in green in Fig. 2). Since the SBDs $\tau_{1-3}$ cannot be changed during the measurement, $TI_3$ is also not changeable during the measurement. As all subjects showed a normal inflow behavior, a late $TI_3$ is therefore not optimal, because here the brain is already perfused to a large extent. Thus, these experiments only served to show that the algorithm reacts accordingly to a change in the start values.

The same is true for the second setting (here $TI_3 = 1820$ ms). Again, the algorithm set the pCASL-$PLD_7$ to the smallest possible value in all subjects. In contrast, a $TI_{max}$ of 2600 ms and $TI_3 = 820$ ms should have resulted in a maximum allowable pCASL-$PLD_7$ of 1600 ms. This was the case only for subject 1 in one of three repetitions. Instead, the algorithm brought the pCASL-$PLD_7$ back to the minimum allowed value of 1520 ms in almost all repetitions and subjects. A plausible reason for this could be that only a small range of 80 ms between the maximum and minimum allowed pCASL-$PLD_7$ could be determined anyway. Therefore, the range may have simply been too small to reliably find the optimal pCASL-$PLD_7$. For comparison, in the selected start setting with $TI_{max} = 3600$ ms, the pCASL-$PLD_7$ could be adapted in a range of 1080 ms.

To further test the robustness and behavior of the proposed algorithm, the constraints for SBDs and pCASL-BD should be adjusted according to the studied start settings to allow for a wider range of adaption. Furthermore, the results of the algorithm could be simulated in future work with artificial PWIs to detect unusual behavior.

## Evaluation of CBF and ATT maps

The quantification results for mean CBF and ATT can be retrieved from Figs. 4, 5.

It can be recognized that the CBF values vary slightly between the ss- and seg-data. For GM in the range of the determined standard deviation, but for WM in a larger degree. The values of ATT, on the other hand, varied almost exclusively in the range of the determined uncertainties. However, more interesting for the evaluation of the algorithm presented here is the difference between the mean CBF and ATT with the respective standard deviation as a measure of the uncertainty of the fit for the different timings. For all subjects, the standard deviations of the adapted timing are within the range of the standard deviations from the recommended timing for healthy humans, while the uncertainty in suboptimal sampling increases significantly especially for the intentionally too-short pCASL-PLD of

1000 ms (pCASL-BD = 2600 ms). This indicates that especially an improper sampling of the inflow curve and a final pCASL-subbolus PWI with ATD artifacts can lead to a poor fit result.

## Analysis of ATD artifacts

As desired, the brain was almost completely perfused in the PWI before the pCASL-PWI (Fig. 6). On visual inspection, the pCASL-PWI of the adapted timing also show no signs of ATD artifacts, except that the results from subject 2 show a hyperintense signal in the outer brain area. This could be due to the rather short pCASL-$PLD_7$ in this subject.

In the results of the intentionally suboptimal timing with pCASL-BD = 2600 ms, hyperintense signal areas are clearly visible in all subjects. Analysis of the image histograms also shows that the difference between mean and median is larger for this suboptimal timing than for the other three timings studied (Fig. 7). Because only healthy subjects were measured in this study, the adjusted data and the data with the recommended pCASL-BD show similar results. On average, the adapted data show a slightly smaller difference, which is mainly due to the fact that the adapted pCASL-$PLD_7$ is slightly longer than 1800 ms for subjects 3, 4, and 5. In contrast, the difference between mean and median is larger for subject 2. Here, the algorithm detected a low pCASL-$PLD_7$ of 1520 ms and one can visually see some hyperintense signals in the outer brain area (Fig. 6). However, Fig. 6 also shows that a pCASL-$PLD_7$ of 1800 ms (pCASL-BD = 1800 ms) would have been too long for subject 2, as the brain seems to be already fully perfused on the PWI before the pCASL-PWI (indicated by red cycle). Therefore, an optimal timing is probably slightly above the determined 1520 ms, at least for the watershed regions. The algorithm consistently determined the minimum possible pCASL-$PLD_7$ in subject 2. The optimal, slightly longer $PLD_7$ was probably not found because of the minimum allowable SBD $\tau_6$.

The difference between the mean and median of the image histogram is even smaller for the second suboptimal timing (pCASL-BD = 1000 ms) than for all other timings (see Fig. 7). This is due to the relatively long pCASL-$PLD_7$ in healthy subjects and the relatively short BD, which also leads to a lower SNR.

## Limitations, optimizations and future applications

The most important limitation of the present study is that only healthy volunteers were scanned. However, this study was designed to test and present the technical solution such an adaptive approach could provide when individual sequence timing adaptions are desired. To assess the clinical value of the adaptive WH-pCASL, studies should be performed in different age groups and in patients. The small number of subjects is sufficient for a technical feasibility study such as the presented.

Moreover, for a detailed statistical analysis of the robustness of the algorithm, more repetitions should be measured in a test–retest design. The algorithm could also be challenged as mentioned by feeding it with different simulated input data. Preliminary tests have shown a robust behavior, but this was not yet studied in detail.

Furthermore, the decision criteria could be optimized or combined with other parameters such as entropy for instance, to find potential ATD artifacts independently of the here presented "number of filled voxels above noise level" rule. Another point of discussion in this context would be the defined threshold as of when a voxel is considered "filled" and when it is not.

In the current implementation of the presented method, the relative difference in NoV between two compared PWIs directly determines the shortening or lengthening of pCASL-BD and SBDs within the predefined constraints. Whether this adjustment could also be based on a different rule will be analyzed in future applications. The predefined SBD constraints could also be modified, although, as in this study, $T_1$ relaxation and SNR constraints when SBDs become too short should always be kept in mind.

In addition to the adjustments of the SBD constraints or the decision criteria when and how much to adjust the SBDs for each acquired matrix row, the presented algorithm offers further theoretical strategies to make the best use of its flexibility. One possible adaptation would be to consider a desired "filling level" of the brain in the intermediate PWIs. At the expense of measurement time, since individual matrix rows would have to be acquired repeatedly more often, a flexible number of iterations at each decision level would be conceivable until a certain "filling level" of the brain is reached at each step.

Motion is a regular problem in time-encoded pCASL and can affect the whole measurement. The method presented does not protect against this and motion artefacts could potentially harm the timing adjustment process. One advantage of the presented approach is that only two rows of the encoding matrix are used to calculate the intermediate PWI in each case. However, patient movement that occurs between these two image acquisitions can corrupt the intermediate PWIs and the final decoding of all PWIs as well. Therefore, it is suggested to perform on-going constituency checks throughout the measurement and a retrospective motion correction before each calculation of the individual intermediate PWIs. Once all matrix rows have been acquired, retrospective motion correction can then be performed again using either the encoded image of the first matrix row or the M0 image as a reference image for registering all encoded images before decoding the

final PWIs. Both methods already work within the implemented online image reconstruction pipeline but were not necessary in this work because the registered motion of the subjects was very low. If too much motion of the images was noticed during image registration, the described method could also be used to trigger a new acquisition of the last matrix row(s). Other prospective motion correction methods without [39] or with external devices [40] might also be applicable in the future.

## Conclusion

The proposed adaptation algorithm for FL WH-pCASL is able to successfully calculate intermediate PWI and adjust sequence timing during active scanning based on individual inflow behavior of labeled blood in time-encoded ASL imaging. The presented acquisition strategy thus allows subject-specific adjustments within predefined limits of ASL parameters such as BD and PLD during an ongoing measurement. In this way, time-encoded ASL can be automatically tailored to an individual subject. The presented method aims to reduce ATD artifacts, improve ASL perfusion quantification results, and avoid reacquisitions in clinical settings. However, the extent to which the results are transferable to patients and provide benefit needs to be investigated in follow-up studies.

**Supplementary Information** The online version contains supplementary material available at https://doi.org/10.1007/s10334-023-01121-y.

**Author contributions** N-JB: study conception and design, acquisition of data, analysis and interpretation of data, drafting of manuscript. DCH: acquisition of data, critical revision. Konstandin: analysis and interpretation of data, critical revision. MAB: acquisition of data, analysis and interpretation of data, critical revision. AM: acquisition of data, analysis and interpretation of data, critical revision. KE: analysis and interpretation of data, critical revision. FvS-H: analysis and interpretation of data, critical revision. MG: study conception and design, analysis and interpretation of data, critical revision. The first draft of the manuscript was written by N-JB and all authors commented on previous versions of the manuscript. All authors read and approved the final manuscript.

**Funding** Open Access funding enabled and organized by Projekt DEAL. Our research is supported by the EU JPND research program (for Germany BMBF grant 01ED2107). The DEBBIE project (Developing a non-invasive biomarker for early BBB breakdown in Alzheimer's disease) is an EU Joint Programme-Neurodegenerative Disease Research (JPND) project. It is supported through the following funding organisations under the aegis of JPND-www.jpnd.eu(FWO in Belgium, Canadian Institutes of Health Research in Canada, BMBF in Germany, NFR in Norway, ZonMw in The Netherlands, TÜBITAK in Turkey). The project has received funding from the European Union's Horizon 2020 research and innovation programme under grant agreement No. 825664.

**Data availability** Upon individual requests, the authors will provide access to the data used accordingly.

## Declarations

**Conflict of interest** The following financial relationships outside of the presented work include the following: mediri GmbH (employee, part-time: MG, SK, KE). For the underlying method, a patent was granted in Germany (DE102016206724) and China (CN109073722B) and patent applications in further legislatures are pending.

**Ethical approval** All subjects provided written, informed consent before scanning and the study was run under a general protocol for pulse-sequence development approved by the local ethics committee (University of Bremen, Germany) in accordance with the Declaration of Helsinki.



## References

1. Williams DS et al (1992) Magnetic resonance imaging of perfusion using spin inversion of arterial water. Proc Natl Acad Sci USA 89(1):212–216. https://doi.org/10.1073/pnas.89.1.212
2. Wang J, Fernandez-Seara MA, Wang S, St Lawrence KS (2007) When perfusion meets diffusion: in vivo measurement of water permeability in human brain. J Cereb Blood Flow Metab 27:839–849. https://doi.org/10.1038/sj.jcbfm.9600398
3. Lin Z et al (2018) Non-contrast MR imaging of blood–brain barrier permeability to water. Magn Reson Med 80:1507–1520. https://doi.org/10.1002/mrm.27141
4. Wong EC, Buxton RB, Frank LR (1998) A theoretical and experimental comparison of continuous and pulsed arterial spin labeling techniques for quantitative perfusion imaging. Magn Reson Med 40(3):348–355. https://doi.org/10.1002/mrm.1910400303
5. Wong EC et al (2006) Velocity-selective arterial spin labeling. Magn Reson Med 55(6):1334–1341. https://doi.org/10.1002/mrm.20906
6. Detre JA et al (1992) Perfusion imaging. Magn Reson Med 23(1):37–45. https://doi.org/10.1002/mrm.1910230106
7. Garcia DM, De Bazelaire C, Alsop DC (2005) Pseudo-continuous flow driven adiabatic inversion for arterial spin labeling. In: Proceedings of the 13th annual meeting of ISMRM (abstract 37)
8. Wong EC (2007) Vessel-encoded arterial spin-labeling using pseudocontinuous tagging. Magn Reson Med 58(6):1086–1091. https://doi.org/10.1002/mrm.21293
9. Dai W et al (2008) Continuous flow-driven inversion for arterial spin labeling using pulsed radio frequency and gradient fields. Magn Reson Med 60(6):1488–1497. https://doi.org/10.1002/mrm.21790

10. Pollock JM et al (2009) Arterial spin-labeled MR perfusion imaging: clinical applications. Magn Reson Imaging Clin N Am 17(2):315–338. https://doi.org/10.1016/j.mric.2009.01.008
11. Wu W-C, St Lawrence KS, Licht DJ, Wang DJJ (2010) Quantification issues in arterial spin labeling perfusion magnetic resonance imaging. Top Magn Reson Imaging 21:65–73. https://doi.org/10.1097/RMR.0b013e31821e570a
12. Zaharchuk G (2012) Arterial spin labeling for acute stroke: practical considerations. Transl Stroke Res 3:228–235. https://doi.org/10.1007/s12975-012-0159-8
13. Petersen ET, Mouridsen K, Golay X (2010) The QUASAR reproducibility study, part II: results from a multi-center arterial spin labeling test-retest study. Neuroimage 49:104–113. https://doi.org/10.1016/j.neuroimage.2009.07.068
14. Buxton RB et al (1998) A general kinetic model for quantitative perfusion imaging with arterial spin labeling. Magn Reson Med 40(3):383–396. https://doi.org/10.1002/mrm.1910400308
15. Alsop DC et al (2015) Recommended implementation of arterial spin-labeled perfusion MRI for clinical applications: a consensus of the ISMRM perfusion study group and the European consortium for ASL in dementia. Magn Reson Med 73(1):102–116. https://doi.org/10.1002/mrm.25197
16. Dai W, Fong T, Jones RN, Marcantonio E, Schmitt E, Inouye SK, Alsop DC (2017) Effects of arterial transit delay on cerebral blood flow quantification using arterial spin labeling in an elderly cohort. J Magn Reson Imaging 45(2):472–481. https://doi.org/10.1002/jmri.25367
17. Bokkers RP, van der Worp HB, Mali WP, Hendrikse J (2009) Noninvasive MR imaging of cerebral perfusion in patients with a carotid artery stenosis. Neurology 73:869–875. https://doi.org/10.1212/WNL.0b013e3181b7840c
18. Mutke MA et al (2014) Clinical evaluation of an arterial-spin-labeling product sequence in steno-occlusive disease of the brain. PLoS ONE 9(2):e87143. https://doi.org/10.1371/journal.pone.0087143
19. Wang R et al (2014) Multi-delay arterial spin labeling perfusion MRI in moyamoya disease—comparison with CT perfusion imaging. Eur Radiol 24(5):1135–1144. https://doi.org/10.1007/s00330-014-3098-9
20. Borogovac A, Asllani I (2012) Arterial spin labeling (ASL) fMRI: advantages, theoretical constrains and experimental challenges in neurosciences. Int J Biomed Imaging 2012:818456. https://doi.org/10.1155/2012/818456
21. Teeuwisse WM et al (2014) Time-encoded pseudocontinuous arterial spin labeling: basic properties and timing strategies for human applications. Magn Reson Med 72(6):1712–1722. https://doi.org/10.1002/mrm.25083
22. Günther M (2007) Highly efficient accelerated acquisition of perfusion inflow series by cycled arterial spin labeling. In: Proceeding of the 15th annual meeting of ISMRM (abstract 380)
23. Wells JA, Lythgoe MF, Gadian DG, Ordidge RJ, Thomas DL (2010) In vivo Hadamard encoded continuous arterial spin labeling (H-CASL). Magn Reson Med 63:1111–1118. https://doi.org/10.1002/mrm.22266
24. Dai W, Shankaranarayanan A, Alsop DC (2013) Volumetric measurement of perfusion and arterial transit delay using hadamard encoded continuous arterial spin labeling. Magn Reson Med 69:1014–1022. https://doi.org/10.1002/mrm.24335
25. Chalela JA, Kidwell CS, Nentwich LM, Luby M, Butman JA, Demchuk AM, Hill MD, Patronas N, Latour L, Warach S (2007) Magnetic resonance imaging and computed tomography in emergency assessment of patients with suspected acute stroke: a prospective comparison. Lancet 369:293–298. https://doi.org/10.1016/S0140-6736(07)60151-2
26. Kuperman JM, Brown TT, Ahmadi ME, Erhart MJ, White NS, Roddey JC, Shankaranarayanan A, Han ET, Rettmann D, Dale AM (2011) Prospective motion correction improves diagnostic utility of pediatric MRI scans. Pediatr Radiol 41:1578–1582. https://doi.org/10.1007/s00247-011-2205-1
27. Zun Z, Shankaranarayanan A, Zaharchuk G (2014) Pseudocontinuous arterial spin labeling with prospective motion correction (PCASL-PROMO). Magn Reson Med 72:1049–1056. https://doi.org/10.1002/mrm.25024
28. von Samson-Himmelstjerna F, Madai VI, Sobesky J, Guenther M (2015) Walsh-ordered hadamard time-encoded pseudocontinuous ASL (WH pCASL). Magn Reson Med 76(6):1814–1824. https://doi.org/10.1002/mrm.26078
29. Dai W, Robson PM, Shankaranarayanan A, Alsop DC (2012) Reduced resolution transit delay prescan for quantitative continuous arterial spin labeling perfusion imaging. Magn Reson Med 67(5):1252–1265. https://doi.org/10.1002/mrm.23103
30. Breutigam NJ, von Samson-Himmelstjerna F, Günther M (2016) Automatic adaption of ASL labeling parameters: Walsh-sorted time-encoded pCASL with a dynamic feedback algorithm. In: Proceedings of the 24th annual meeting ISMRM (abstract 1000)
31. Breutigam NJ, Buck MA, Hoinkiss DC, von Samson-Himmelstjerna F, Günther M (2019) Automated subject-specific adaption of pCASL timing parameters in real time. In: Proceedings of the University of Michigan International Workshop on arterial spin labeling MRI: technical updates and clinical experience (abstract 27)
32. Breutigam NJ, Hoinkiss DC, Buck MA, Mahroo A, von Samson-Himmelstjerna F, Guenther M (2020) Optimal subject-specific pCASL settings by automated inner-scan timing adaption. In: Proceedings of the 28th annual meeting of the ISMRM (abstract 3282)
33. Guenther M, Oshio K, Feinberg DA (2005) Single-shot 3D imaging techniques improve arterial spin labeling perfusion measurements. Magn Reson Med 54(2):491–498. https://doi.org/10.1002/mrm.20580
34. Silver M, Joseph R, Hoult D (1984) Highly selective and π pulse generation. J Magn Reson 59:347–351. https://doi.org/10.1016/0022-2364(84)90181-1
35. Chappell MA, Groves AR, Whitcher B, Woolrich MW (2009) Variational Bayesian inference for a non-linear forward model. IEEE Trans Signal Process 57(1):223–236. https://doi.org/10.1109/TSP.2008.2005752
36. Amukotuwa SA, Yu C, Zaharchuk G (2016) 3D pseudocontinuous arterial spin labeling in routine clinical practice: a review of clinically significant artifacts. J Magn Reson Imaging 43(1):11–27. https://doi.org/10.1002/jmri.24873
37. Alisch JSR et al (2021) Sex and age-related differences in cerebral blood flow investigated using pseudo-continuous arterial spin labeling magnetic resonance imaging. Aging (Albany NY) 13(4):4911–4925. https://doi.org/10.18632/aging.202673
38. Mahroo A, Buck M, Huber J, Breutigam N-J, Mutsaerts H, Craig M, Chappell M, Günther M (2021) Robust multi-TE ASL-based blood–brain barrier integrity measurements. Front Neurosci 15:719676. https://doi.org/10.3389/fnins.2021.719676
39. Kouwe A, Andre J (eds) (2022) Motion correction in MR, part 7. Advances in magnetic resonance technology and applications, vol 6. Elsevier. ISSN: 2666-9099. ISBN: 9780128244609
40. Madore B, Hess AT, van Niekerk AMJ, Hoinkiss DC, Hucker P, Zaitsev M, Afacan O, Günther M (2022) External hardware and sensors for improved MRI. J Magn Reson Imaging 57(3):690–705. https://doi.org/10.1002/jmri.28472